



CHORUS

This is the accepted manuscript made available via CHORUS. The article has been published as:

Nonequilibrium polarization dynamics in antiferroelectrics

M. M. Vopson and X. Tan

Phys. Rev. B **96**, 014104 — Published 7 July 2017

DOI: [10.1103/PhysRevB.96.014104](https://doi.org/10.1103/PhysRevB.96.014104)

Non-equilibrium polarization dynamics in anti-ferroelectrics

M.M. Vopson^{1*}♦, X. Tan²

^{1*} Faculty of Science, SEES, University of Portsmouth, Portsmouth PO1 3QL, UK.

² Department of Materials Science and Engineering, Iowa State University, Ames, Iowa 50011, USA.

* Correspondence to: melvin.vopson@port.ac.uk; ♦ Formerly known as Vopsaroiu

A **non-equilibrium statistical** domain nucleation model of polarization dynamics in less understood anti-ferroelectric systems is introduced. Predictions of the model have been successfully tested experimentally using an anti-ferroelectric $\text{Pb}_{0.99}\text{Nb}_{0.02}[(\text{Zr}_{0.57}\text{Sn}_{0.43})_{0.94}\text{Ti}_{0.06}]_{0.98}\text{O}_3$ polycrystalline ceramic. We determined the activation energy of the domain nucleation process for this particular anti-ferroelectric sample to be $W_b = 1.07$ eV and the critical volume of the polar nucleus $V^* = 98 \times 10^{-27}$ m³, which corresponds to a linear length scale of 2.86 nm.

1. Introduction

Anti-ferroelectric materials were first predicted by Kittel in 1951 using Landau-Devonshire phenomenological theory [1] and shortly confirmed experimentally in PbZrO_3 ceramics [2,3]. Anti-ferroelectrics display a field induced transition from antipolar to polar dielectric and they have interesting properties such as the double hysteresis loop and large strains associated with it. These unique properties make anti-ferroelectric materials very attractive for technological applications involving high-energy super-capacitors [4-8], electro-caloric cooling [9], actuators [10], photovoltaic effects [11] and many other interesting dielectric phenomena. Very recently, experimental evidence of a novel 4-state non-volatile memory effect in anti-ferroelectrics has been reported [12]. A similar non-volatile memory effect, but fundamentally different to the previously reported one was published by Pesic et al. [13]. These simultaneous and independent studies concluded the possibility of utilizing anti-ferroelectric materials for non-volatile random access memory (RAM) chips called AFRAM [14]. The AFRAM memories bring considerable improvements to ferroelectric RAM, FRAM [15-19], while maintaining key features of FRAM such as low power consumption, ultra-fast data accesses times and read / write endurance of $> 10^{12}$. These discoveries and proposed applications can only be turned into commercial products if the temperature, time and electric field dependence of the polarization dynamics in anti-ferroelectrics are fully understood. Unfortunately, anti-ferroelectrics are complex systems and, despite major scientific advances [20-23], there is no clear understanding of their polarization dynamics.

The situation is rather different with ferroelectric materials, where the theories of polarization dynamics are well established and better understood. The wider consensus is that polarization reversal in ferroelectrics takes place via a nucleation of domains and the movement of domain walls, which subsequently expand and grow at the expense of the existing domains [24-29]. A simple phenomenological description of the polarization dynamics in ferroelectrics was given by Kolmogorov-Avrami-Ishibashi (KAI) domain nucleation-switching model [30-35] and subsequent variants of it [36-38]. KAI model assumes that the application of an electric field generates nuclei of reversed polarization and the polarization switching involves 4 steps: i) nucleation of domains; ii) rapid growth of nuclei along polarization direction; iii) sidewise growth of the domains; iv) coalescence of the domains until full polarization reversal is completed. Despite being able to successfully describe polarization kinetics of ferroelectric single crystals [30] and some epitaxial thin films [39], KAI model is very limited in applicability because of its failure to predict the relationship between the switching time to the applied electric field and temperature [36,40]. Various attempts to

Confidential

modify the KAI model in order to increase its applicability were made by assuming a distribution of relaxation times [37], a nucleation limited switching model [36] and a statistical time dependent depolarization field [38]. However, just as the KAI model, these variants still lack the full analytical inclusion of electric field, time and temperature dependence of the reversed polarization and switching time. By assuming a domain nucleation mechanism of polarization switching and applying a non-equilibrium statistical model to describe the time dependent polarization reversal probability of nano-polar regions, with a critical volume V^* , Vopsaroiu et al. [41] were able to fully solve these deficiencies [*Phys. Rev. B*, 82, 024109 (2010)] **and fully reproduce the KAI equations. However, unlike the KAI model, this approach** successfully accounted for the applied electric field, time and temperature contributions to produce comprehensive analytical relations for the reversed polarization, switching time, switching current and coercive field [41], but also domain wall velocity, Curie law in ferroelectrics [42] and lattice mismatch strain/stress effects [43]. Given that anti-ferroelectrics consist of two equally and opposing ferroelectric sublattices, in this paper we examine the physics of polarization dynamics in anti-ferroelectric materials, using Vopsaroiu's non-equilibrium domain nucleation model applied to each ferroelectric sublattice.

2. Anti-ferroelectric double hysteresis loop explained

Figure 1 shows a typical anti-ferroelectric double hysteresis loop. We shall refer to the two ferroelectric sublattices of the anti-ferroelectric as sublattice A and sublattice B. In this convention, at zero applied electric field, sublattice A has negative polarization $P_A = -P_s$ and sublattice B has positive polarization, $P_B = +P_s$, where P_s is the absolute saturation polarization / spontaneous polarization of each sublattice. Hence, when the applied E field is zero, the anti-ferroelectric has zero polarization due to the self-cancellation of the macroscopic polarizations of the two consisting ferroelectric sublattices, $P = P_A + P_B = 0$, as seen in figure 1. This is also well represented schematically in figure 2.a), which shows the zero polarization state and the unit cells of the ferroelectric sublattices A and B, at equilibrium, and under no applied external field. The application of a large enough positive or negative external electric field results in switching of the anti-ferroelectric from antipolar to polar ferroelectric. Therefore, under the influence of an applied electric field, the anti-ferroelectric displays a double hysteresis (see figure 1), with each hysteresis loop representing the response of the induced ferroelectric phase with

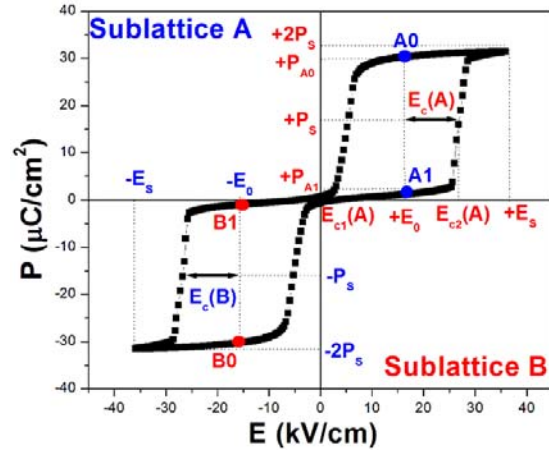


Figure 1. Typical anti-ferroelectric double hysteresis loop with the main parameters marked on it.

polarization in the direction of one of the two sublattices. Hence, a positive applied field, $+E$, would result in the reversal of the negative sublattice A, while leaving the positive sublattice B unaffected (see figure 2.d,e). Therefore, the hysteresis loop in the positive quadrant of figure 1 corresponds to the reversal of the negative sublattice A. Similarly, a negative applied field, $-E$, would result in the reversal of the positive sublattice B (figure 2.b,c) and the negative hysteresis loop in figure 1 corresponds to the reversal of the positive sublattice B. In order to explain the polarization dynamics of anti-ferroelectrics and to formulate the theoretical model, we make the following notations on the double hysteresis loop: $E_c(A) = E_0 - E_{c1}(A) = E_{c2}(A) - E_0$ is the coercive field of the sublattice A;

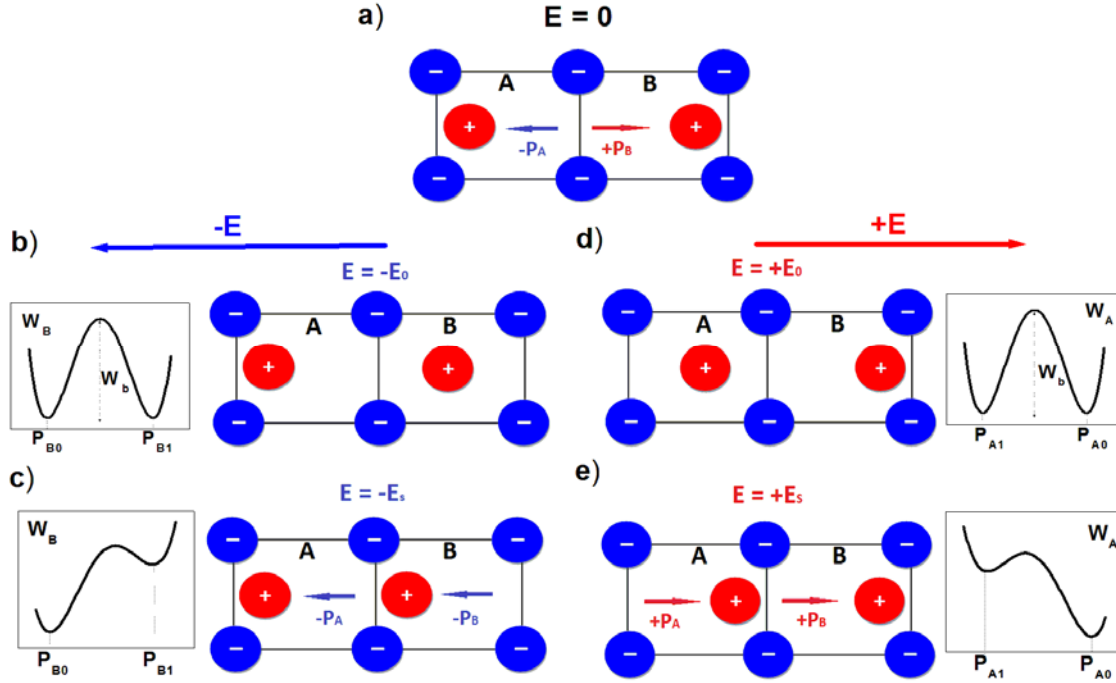


Figure 2. Schematic diagram of the unit cells of a hypothetical anti-ferroelectric material consisting of ferroelectric sublattices A and B, respectively. a) Anti-ferroelectric in ground state at $E = 0$, $P = 0$; b) Reversal of the positive sublattice B under the action of negative E field, while A sublattice remains unchanged. At E field equal to the critical activation field, $E = -E_0$, the free energy of the sublattice B shows two equally probable energy states corresponding to P_{B0} and P_{B1} ; c) At saturating negative field $E = -E_s$, the sublattice B is fully reversed; d) Reversal of the negative sublattice A under the action of positive E field, while B sublattice remains unchanged. When $E = +E_0$, the free energy of the sublattice A shows two equally probable energy states corresponding to P_{A0} and P_{A1} ; e) When $E = +E_s$, the negative sublattice A is fully reversed into positive polarization;

$E_c(B) = -E_0 - E_{c1}(B) = E_{c2}(B) - E_0$ is the coercive field of the sublattice B; $\pm E_s$ are the positive and negative saturation electric fields; $\pm 2P_s$ are the positive and negative saturation polarization values of the whole anti-ferroelectric sample; $\pm P_s$ are the positive and negative saturation polarization values of each ferroelectric sublattice; $\pm E_0$ are the activation fields at which the hysteresis loops are centred, and they are equivalent to $E = 0$ axis of the hysteresis loop of a ferroelectric material; $+E_0$ intersects the positive hysteresis loop of the sublattice A at points A0 and A1; $-E_0$ intersects the negative hysteresis loop of the positive sublattice B at points B0 and B1; The meaning of A0, A1, B0 and B1 is that of pseudo-remnant polarization states (see figure 1) that can be accessed only when the system is excited at the critical fields $\pm E_0$. $+P_{A0}$ and $+P_{A1}$ are the upper and lower pseudo-remnant polarization states of the sublattice A, and $-P_{B0}$ and $-P_{B1}$ are the upper and lower pseudo-remnant polarization states of the sublattice B, respectively (figure 1 and 2).

3. Theory

Having the parameters of the double hysteresis loop defined, we now recall that polar ferroelectric materials display a single hysteresis loop and they can be described using Landau – Devonshire formalism in terms of their free energy expansion around the order parameter. The free energy function has two equilibrium minima corresponding to the two possible remanent polarization states of a ferroelectric system, separated by an energy barrier, W_b . At $E = 0$, the two possible states are equally probable and reversal from one state to another can only take place if an energy comparable to W_b is supplied to the system. An applied E field will distort the balance of probabilities and will promote the reversal into one of the two states, depending on the polarity of the applied E field. This is the correct description of the polarization reversal process at $T = 0K$. If $T \neq 0K$, then an additional Boltzmann energy term, $k_B T$, will contribute to the reversal process. In fact, at $T \neq 0K$, there is a non-zero probability that reversal over W_b occurs even at $E = 0$, leading to spontaneous polarization reversal. The ferroelectric is essentially a non-equilibrium system in which nucleation polar sites undergo statistical transitions between the two physically permitted states on a continuous basis, and the occupation probabilities \wp_l and \wp_m of two possible states are also time dependent (throughout the paper “ \wp ” refers to occupation probability and “ P ” refers to electric polarization). The time evolution of the probabilities when a non-equilibrium system goes through different possible states are described by the general Pauli-Master equation [44]:

$$\frac{d\wp_l}{dt} = \sum_{m \neq l} (a_{l,m}\wp_m(t) - a_{m,l}\wp_l(t)) \quad (1)$$

where: $1 \leq l, m \leq \Omega$ with l and m taking integer values and Ω is the number of possible states of the system compatible with the macro-state; $\wp_l(t)$ and $\wp_m(t)$ are the probabilities that the system is in the state l or m at the time t , respectively; $a_{l,m}$ and $a_{m,l}$ are the transition rates per unit time from the state m to state l and vice versa, respectively. For a system in contact with a temperature reservoir, T , the pseudo-symmetry relation between the transition rates is:

$$a_{l,m} e^{-(W_m / k_b T)} = a_{m,l} e^{-(W_l / k_b T)} = \nu_0 \quad (2)$$

where W_m and W_l are the energies in the state m and l , respectively and ν_0 is a constant equal to the total number of trials per second to overcome the energy barrier, taken as the frequency of the optical phonons in the crystal $\sim 10^{13}$ Hz [38]. Since ferroelectrics are systems with two energy minima states, the equation (1) has been solved for $\Omega = 2$ (i.e. a two state system) for which $l, m = 1, 2$ [41,42]. In the case of anti-ferroelectrics, the occurrence of the double hysteresis loop implies that there are two meta-stable equilibrium states for each ferroelectric sublattice, with a total of four meta-stable equilibrium states corresponding to points A0, A1, B0 and B1, respectively (figure 1). This corresponds to $\Omega = 4$ in equation (1) while the polarization values of these four meta-stable states are P_{A0} , P_{A1} , P_{B0} and P_{B1} respectively, having the meaning of pseudo-remanent polarizations that occur at the critical activation fields $\pm E_0$. Assuming non-interacting nucleation nano-polar sites within each ferroelectric sublattice, then we can apply Vopsaroiu’s non-equilibrium domain nucleation model to each ferroelectric sublattice, so that instead of $\Omega = 4$ in equation (1) resulting in a system of 4 differential equations, the problem can be solved as two independent systems of two differential equations, corresponding to $\Omega_A = 2$ and $\Omega_B = 2$, respectively. We now refer to figure 2 where the free energy of each sublattice at $\pm E_0$ and $\pm E_s$ has been plotted as a function of the polarization of each sublattice. The energy of states A0 and A1 within sublattice A are:

$$W_{A0} = -W_b + P_{A0}(E - E_0) \quad (3)$$

Confidential

$$W_{A1} = -W_b + P_{A1} \cdot (E - E_0)$$

It can be easily noticed that if the applied electric field $E = +E_0$, then $W_{A0} = W_{A1} = -W_b$, as seen in figure 2.d. Similarly, the energy of states B0 and B1 within sublattice B are:

$$\begin{aligned} W_{B0} &= -W_b + P_{B0} \cdot (E + E_0) \\ W_{B1} &= -W_b + P_{B1} \cdot (E + E_0) \end{aligned} \quad (4)$$

Hence, if the applied electric field $E = -E_0$, then $W_{B0} = W_{B1} = -W_b$, as seen in figure 2.b. Hence, at $E = \pm E_0$, the two states A0, A1 and B0, B1 are equally probable. Let $\wp_{A0}(t)$ and $\wp_{A1}(t)$ be the probabilities that the sublattice A is at time t in state A0 and A1, and $\wp_{B0}(t)$ and $\wp_{B1}(t)$ are the probabilities that the sublattice B is at time t in state B0 and B1, respectively. Solving the Pauli – Master equation (1) for each sublattice requires identical approach with the exception that the hysteresis loop of the sublattice A is centred at $+E_0$, and the energy of the states A0 and A1 are given by relations (3), while the sublattice B has an activation field $-E_0$ and the energy of states B0 and B1 are given by relations (4). In what follows we are restricting the analysis to sublattice A, bearing in mind that a similar treatment can be applied to sublattice B, by properly considering the energy states and the polarity of the activation field. Solutions of the Pauli – Master equation (1) for sublattice A are:

$$\wp_{A0}(t) = e^{-\left(\frac{t}{t_{sw}}\right)} + \wp_{A0}(\infty) \cdot \left(1 - e^{-\left(\frac{t}{t_{sw}}\right)}\right) \quad (5)$$

$$\wp_{A1}(t) = -e^{-\left(\frac{t}{t_{sw}}\right)} + \wp_{A0}(\infty) \cdot \left(e^{\frac{W_{A1}-W_{A0}}{k_b T}} + e^{-\left(\frac{t}{t_{sw}}\right)}\right) \quad (6)$$

where $\wp_{A0}(\infty)$ is the equilibrium probability of state A0 when $t \rightarrow \infty$. Using (3) and the normalization condition $\wp_{A0}(t) + \wp_{A1}(t) = 1$, $\wp_{A0}(\infty)$ becomes:

$$\wp_{A0}(\infty) = \left(1 + e^{\frac{W_{A1}-W_{A0}}{k_b T}}\right)^{-1} = \left(1 + e^{\frac{(E-E_0)(P_{A1}-P_{A0})}{k_b T}}\right)^{-1} \quad (7)$$

t_{sw} is the polarization switching time at an arbitrary applied E field, given by:

$$t_{sw} = \frac{1}{V_0} \cdot e^{-\left(\frac{W_{A0}}{k_b T}\right)} = \frac{1}{V_0} \cdot e^{\frac{W_b - P_{A0}(E - E_0)}{k_b T}} \quad (8)$$

At the coercive field of the sublattice A, $E_c(A) = E_0 - E_{c1}(A) = E_{c2}(A) - E_0$ (see figure 1), the occupation probabilities of states A0 and A1 are equal because the polarization of the sublattice A is zero ($P_A = 0$) and the polarization of the whole anti-ferroelectric sample is $P = P_A + P_B = +P_s$ (see figure 1 and 2). This implies that when $E = E_c(A)$, then $\wp_{A0}(t) = \wp_{A1}(t)$ and since $\wp_{A0}(t) + \wp_{A1}(t) = 1$, we deduce that $\wp_{A0}(t) = \wp_{A1}(t) = 0.5$ at the coercive field. Using this condition in (5) and (8) and imposing $\wp_{A0}(\infty) \rightarrow 0$ at $E \geq E_c(A)$, after some algebraic re-arrangement we obtain the coercive field of the sublattice A as:

$$E_{c_2}(A) = E_0 + \frac{W_b}{2P_s} - \frac{k_b T}{V^* 2P_s} \cdot \ln\left(\frac{v_o t}{\ln(2)}\right) \quad (9)$$

V^* is the volume of the polar embryo and it comes from the fact that the energies expressed in (2) – (8) are in fact energies per unit volume. Since the equations refer to the total energy, all energy terms must be multiplied with V^* , which has been omitted for convenience. Similarly, the coercive field of the sublattice B is derived as:

$$E_{c_2}(B) = -E_0 - \frac{W_b}{2P_s} + \frac{k_b T}{V^* 2P_s} \cdot \ln\left(\frac{v_o t}{\ln(2)}\right) \quad (10)$$

The equations (9) and (10) describing the coercive field of sublattice A and B as a function of the applied electric field, temperature, time and activation energy barrier of the nucleation process, allow quick testing of the proposed model against experimental data extracted from polarization hysteresis loops.

It is important to mention that in this approach there is no need to specify the form of the Landau – Devonshire free energy, as all contributions and interactions are captured in the energy barrier term, W_b . In fact, any additional energy terms could be specifically considered in the Landau – Devonshire free energy, including depolarizing energy [41] or interfacial stress/strain [43], without compromising this approach. However, it is widely accepted that the depolarizing fields are only significant in thin film structures and negligible in bulk [45], especially bulk anti-ferroelectrics, as in this study. Hence, the present approach neither requires the inclusion of these effects, nor are they relevant for the current study. In this non-equilibrium statistical approach we also do not specify the exact location of the nucleation sites, which could be at special sites where the presence of defects or residual anti-parallel domains could lower the activation energy barrier. Although beyond the scope of this work, in future studies, a more detailed approach could incorporate these effects as well as additional local fields, distribution of fields, distribution of volumes of the nucleation sites and other energy terms, in order to extract additional information from the measurements.

4. Experiments and results

To test the model a ceramic anti-ferroelectric sample $\text{Pb}_{0.99}\text{Nb}_{0.02}[(\text{Zr}_{0.57}\text{Sn}_{0.43})_{1-y}\text{Ti}_y]_{0.98}\text{O}_3$ with $y = 0.06$ (code name PNZST 43/6/2) has been synthesized. Powders of PbO , ZrO_2 , SnO_2 , TiO_2 and Nb_2O_5 with purity levels $>99.9\%$ were batched with an additional 5 wt.% PbO to compensate for PbO evaporation during calcination and sintering. Calcination was repeated twice at 935°C for 4 h for compositional homogeneity. The powder was milled for 7 h in ethanol with zirconia media, dried and pressed. After a final milling of 15 h, 40 g of dried PNZST 43/6/2 powder with acrylic binder was pressed at 75 MPa. Cold isostatic pressing was then applied to the green compact at 400 MPa. After the binder was burnt out at 450°C , sintering was carried out at 1325°C for 3 h. To further increase the density of the ceramic, hot isostatic pressing was carried out at 1150°C and 200 MPa for 2 h in a 20% O_2 , 80% Ar atmosphere. Transmission

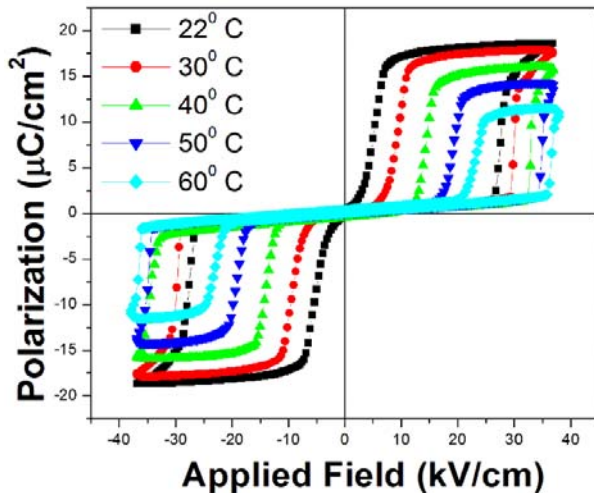


Figure 3. Polarization hysteresis loops as a function of temperature for PNZST 43/6/2 anti-ferroelectric sample.

electron microscopy (TEM) was used to analyse the microstructure of the as-processed ceramic. TEM specimens were prepared via mechanical dimpling and an argon ion mill. Domain morphology and incommensurate modulations were imaged with a Phillips CM-30 TEM operating at 300 kV. Polarization hysteresis loops were acquired using an AiXact Piezo-test Analyser 2000E which was equipped with a sample heating stage and temperature controller in order to perform sample measurements as a function of temperature. The sample used for the polarization measurement is a ceramic disk of 10 mm diameter and 500 μm thickness with metallic electrodes applied on each side of the ceramic disk. Hysteresis loops were acquired using a triangular field waveform of frequency 0.1 Hz and 1.8 kV amplitude with a pre-polarization pulse applied first. Due to the large applied voltages, measurements were only possible at low < 1 Hz frequencies. We observed no significant changes in the double hysteresis loops when measurements were taken at 0.05, 0.1, 0.2 and 0.5 Hz, respectively. The switching current range was 1 mA for this particular sample and experimental conditions. Figure 3 shows the double hysteresis loops measured at room temperature and elevated temperatures ranging from 22° C to 60° C. Although our system allows testing up to 600° C, measurements at higher temperatures were not possible because of multiple cracks and physical sample damage emerging at temperatures above 60° C. From the double hysteresis loop at room temperature we extracted the following parameters of the PNZST 43/6/2 anti-ferroelectric sample: $2P_s = 37.4 \mu\text{C}/\text{cm}^2$, $P_A = |P_B| = P_s = 18.7 \mu\text{C}/\text{cm}^2$, $\pm E_0 = 16.6 \text{ kV}/\text{cm}$ and $\pm E_s = 36 \text{ kV}/\text{cm}$. The electric coercive field was extracted by averaging the $E_c(A)$ from relations: $E_c(A) = E_0 - E_{c1}(A)$ and $E_c(A) = E_{c2}(A) - E_0$, for sublattice A. The same values, but with opposite sign, are obtained for the coercive field of the sublattice B. Figure 4 shows the dependence of the experimental $E_c(A)$ values on the measurement temperature. The equation (9) predicts that the $E_c(A)$ has a theoretical maximum value at $T = 0\text{K}$, and then it decreases linearly with a negative slope as the temperature increases. Remarkably, this is exactly what has been observed experimentally, which has enabled us to perform a theoretical fit to the experimental data using equation (9). The theoretical fit using the linear function $E_c(A) = A - B \cdot T$, resulted in $A = 47.11 \text{ kV}/\text{cm}$ and $B = 0.121$

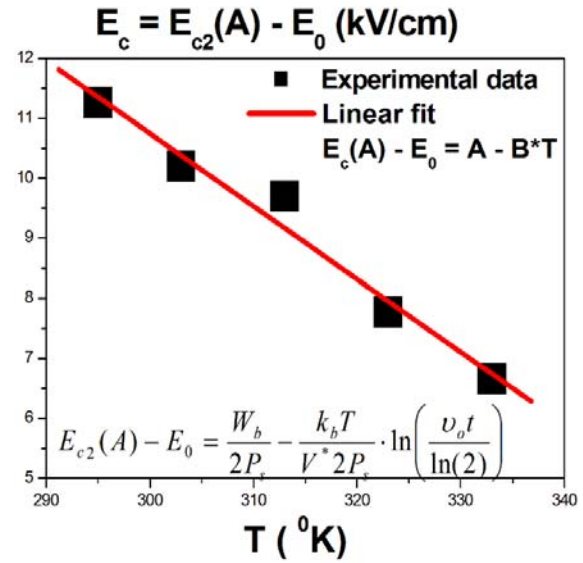


Figure 4. Experimental and theoretical fit of the coercive field values of sublattice A as a function of temperature. The theoretical equation (9) has been used to fit the experimental data.

Figure 3 shows the double hysteresis loops measured at room temperature and elevated temperatures ranging from 22° C to 60° C. Although our system allows testing up to 600° C, measurements at higher temperatures were not possible because of multiple cracks and physical sample damage emerging at temperatures above 60° C. From the double hysteresis loop at room temperature we extracted the following parameters of the PNZST 43/6/2 anti-ferroelectric sample: $2P_s = 37.4 \mu\text{C}/\text{cm}^2$, $P_A = |P_B| = P_s = 18.7 \mu\text{C}/\text{cm}^2$, $\pm E_0 = 16.6 \text{ kV}/\text{cm}$ and $\pm E_s = 36 \text{ kV}/\text{cm}$. The electric coercive field was extracted by averaging the $E_c(A)$ from relations: $E_c(A) = E_0 - E_{c1}(A)$ and $E_c(A) = E_{c2}(A) - E_0$, for sublattice A. The same values, but with opposite sign, are obtained for the coercive field of the sublattice B. Figure 4 shows the dependence of the experimental $E_c(A)$ values on the measurement temperature. The equation (9) predicts that the $E_c(A)$ has a theoretical maximum value at $T = 0\text{K}$, and then it decreases linearly with a negative slope as the temperature increases. Remarkably, this is exactly what has been observed experimentally, which has enabled us to perform a theoretical fit to the experimental data using equation (9). The theoretical fit using the linear function $E_c(A) = A - B \cdot T$, resulted in $A = 47.11 \text{ kV}/\text{cm}$ and $B = 0.121$

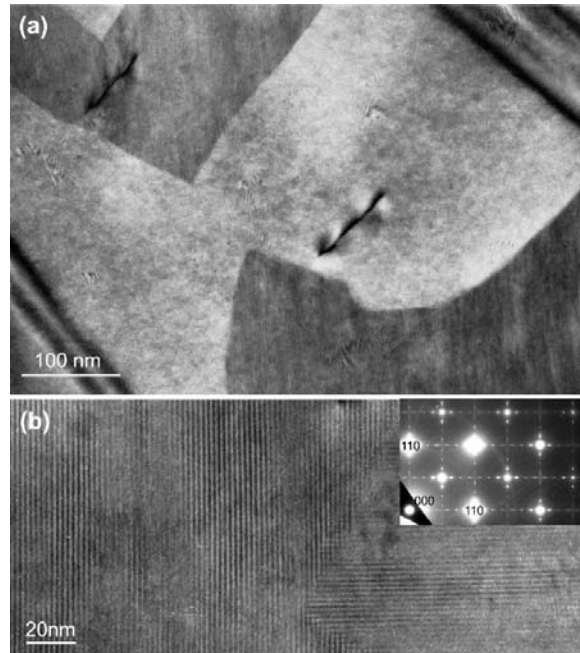


Figure 5. Representative microstructure in the PNZST 43/6/2 ceramic. (a) The anti-ferroelectric 90° domains. (b) The thin 180° domain slabs. The inset in (b) displays the corresponding selected area electron diffraction pattern.

kV/cm·K fitting values. Combining (9) with the linear fitting results we obtain by identification

$$B = \frac{k_b}{V^* 2P_s} \cdot \ln\left(\frac{v_0 t}{\ln(2)}\right).$$

The meaning of t is the fraction of the measurement time taken from the saturating applied electric field to the coercive field. Since the measurements are performed at 0.1 Hz, then the measurement time for the whole double hysteresis loop is 10 seconds, which is split in 5 seconds per sublattice hysteresis loop. Hence, the estimated time is $t = 2.5$ seconds. Taking $v_0 = 10^{13}$ Hz, $k_b = 1.38 \times 10^{-23}$ J/K, $2P_s = 37.4 \mu\text{C}/\text{cm}^2$, and $B = 0.121$ kV/cm·K from the fitting, we determined the volume of the nucleation nano-polar region to be $V^* = 98 \times 10^{-27}$ m³. This corresponds to a linear length scale of 2.86 nm for the polar phase. Similarly, the intercept $A = W_b/2P_s = 47.11$ kV/cm allowed us to calculate the energy barrier $W_b = 2P_s \cdot A \cdot V^* = 1.07$ eV. The meaning of this energy barrier is the activation energy of the polarization reversal of the ferroelectric sublattice at the activation $\pm E_0$ field.

The theoretically estimated critical size of the polar phase is in good agreement with the microstructure analysis of the PNZST 43/6/2 ceramic. Figure 5 displays the typical domain morphology and incommensurate modulations in a grain imaged along the [001] zone-axis. According to previous studies [46], the patches in Fig. 5(a) are anti-ferroelectric 90° domains. Within each 90° domain are the thin 180° domains, which appear as fringes in bright-field images. Figure 5(b) shows these fringes across a 90° domain wall where vertical fringes are seen in the left part of the micrograph and horizontal fringes are seen in the lower-right part. The corresponding selected area diffraction pattern in the inset shows satellite diffraction spots with an incommensurate number of 7.20 [46]. This indicates a wavelength of 2.09 nm, consistent with the fringe spacing directly measured from the bright-field micrograph. According to our previous model for anti-ferroelectric domains [46], the average thickness of the 180° domain slabs is then around 1 nm. Therefore, the theoretically estimated critical size of ~ 2.8 nm is very reasonable. Once one or two slabs of 180° domains are reversed, the critical size is reached and the polar phase can grow further under applied electric field. The coexistence of anti-ferroelectric and ferroelectric domains are clearly identified in the TEM bright field micrographs of anti-ferroelectric PNZST 43/6/2.

5. Conclusions

A domain nucleation non-equilibrium statistical model has been applied to explain the polarization dynamics of anti-ferroelectric materials. A suitable anti-ferroelectric $\text{Pb}_{0.99}\text{Nb}_{0.02}[(\text{Zr}_{0.57}\text{Sn}_{0.43})_{0.94}\text{Ti}_{0.06}]_{0.98}\text{O}_3$ ceramic sample has been fabricated, which allowed experimental confirmation of the model's theoretical predictions. The model and the experimental evidence suggest that polarization reversal in anti-ferroelectrics takes place via a domain nucleation process within each ferroelectric sublattice. The process is triggered in nucleation sites by forming nano-meter-sized polar phase. Using the theoretical model together with the experimental data, we calculated the average volume of the nucleation polar phase to be $V^* = 98 \times 10^{-27}$ m³. This is equivalent to a linear length scale of 2.86 nm. We also determined that the energy barrier of the nucleation polar phase polarization reversal within each sublattice is $W_b = 1.07$ eV, at the activation field $\pm E_0$. These results advance our understanding of anti-ferroelectrics, a class of increasingly important materials, and facilitate their adequate theoretical modelling, fabrication and applications design.

References

- [1] C. Kittel, Phys. Rev. 82: 729–732 (1951)
- [2] G. Shirane, Phys. Rev. vol. 86, No. 2, pp. 219-227 (1952)

Confidential

- [3] E. Sawaguchi, Journal of the Physical Society of Japan, vol. 8, No. 5, pp. 615-629 (1953)
- [4] X. Tan, S.E. Young, Y.H. Seo, J.Y. Zhang, W. Hong, K.G. Webber, Acta Materialia 62, 114–121 (2014)
- [5] X. Hao, Y. Wang, L. Zhang, L. Zhang, S. An, Appl. Phys. Lett. 102, 163903 (2013)
- [6] M.S. Mirshekarloo, K. Yao, T. Sritharan, Appl. Phys. Lett. 97, 142902 (2010)
- [7] A. Chauhan, S. Patel, R. Vaish, C.R. Bowen, Materials 8, 8009–8031(2015)
- [8] Jun Ge, Denis Remiens, Xianlin Dong, Ying Chen, Jean Costecalde, Feng Gao, Fei Cao, Genshui Wang, Appl. Phys. Lett. 105, 112908 (2014)
- [9] A.S. Mischenko, Q. Zhang, J.F. Scott, R.W. Whatmore, N.D. Mathur, Science 311, 1270 (2006)
- [10] S.T. Zhang, A. B. Kounga, W. Jo, C. Jamin, K. Seifert, T. Granzow, J. Rodel, D. Damjanovic, Adv. Mater. 21, 1 (2009)
- [11] A.P. Tomas, M.L. Cnatu, G. Catalan, Adv. Mater. Vol. 28, 9644-9647 (2016)
- [12] M.M. Vopson, G. Caruntu, X. Tan, Scripta Materialia, vol.128, 61-64 (2017)
- [13] M. Pešić, M. Hoffmann, C. Richter, T. Mikolajick, U. Schroeder, Adv. Funct. Mater. Vol. 26, Issue 41, pg. 7486–7494 (2016)
- [14] M.M. Vopson, X. Tan, IEEE Electron Device Letters, vol. 37, No. 12, 1151-1554 (2016)
- [15] H. Ishiwara, Ferroelectric Random Access Memories, J. Nanosci. Nanotechnol. 12, 7619–7627, (2012)
- [16] A. Sheikholeslami, P.G. Gulak, A survey of circuit innovations in ferroelectric random-access memories, Proceedings of the IEEE, vol. 88, No. 5 (2000).
- [17] J.F. Scott, A comparison of magnetic random access memories and ferroelectric random access memories, Struct. Bond. 124, 199-207 (2007).
- [18] R. Guo, L. You, y. Zhou, Z.S. Lim, X. Zou, L. Chen, R. Ramesh, J. Wang, Non-volatile memory based on the ferroelectric photovoltaic effect, Nature Communications 4:1990 (2013).
- [19] Y. Kato, Y. Kaneko, H. Tanaka, K. Kaibara, S. Koyama, K. Isogai, T. Yamada, Y. Shimada, *Overview and future challenge of ferroelectric random access memory technologies*. Jpn. J. Appl. Phys. 46, 2157 (2007).
- [20] A.K. Tagantsev, K. Vaideeswaran, S.B. Vakhrushev, A.V. Filimonov, R.G. Burkovsky, A. Shaganov, D. Andronikova, A.I. Rudskoy, A.Q.R. Baron, H. Uchiyama, D. Chernyshov, A. Bosak, Z. Ujma, K. Roleder, A. Majchrowski, J.-H. Ko, N. Setter, NATURE COMMUNICATIONS, 4:2229 (2013)
- [21] X. Hao, J. Zhai, L.B. Kong, Z. Xu, Prog. Mater. Sci. 63, 1 (2014)
- [22] H. Guo, X. Tan, Phys. Rev. B 91, 144104 (2015)
- [23] I.B. Misirlioglu, L. Pintilie, K. Boldyreva, M. Alexe, D. Hesse, Appl. Phys. Lett. 91, 202905 (2007)
- [24] W. J. Merz, (1954) Phys. Rev. 95 690
- [25] D. Berlincourt, H.A. Krueger, J. Appl. Phys. 30, 1804 (1959)
- [26] D. Damjanovic Rep. Prog. Phys. 61 (1998) 1267 – 1324
- [27] R. Landauer, J. Appl. Phys. 28, 227 (1957)
- [28] An-Quan Jian, H.J. Lee, C.S. Hwang, T.A. Tang, 1954 Phys. Rev. B 80, 0204119 (2009)
- [29] L. Tian, D.A. Scrymgeour, V. Gopalan, Journal of Applied Physics 97, 1141111 (2005)
- [30] S. Hashimoto, H. Orihara, Y. Ishibashi, J. Phys. Soc. Jpn. 63, 1601 (1994)
- [31] H. Orihara, S. Hashimoto, Y. Ishibashi, J. Phys. Soc. Jpn. 63, 1031 (1994)
- [32] A.N. Kolmogorov, Izv. Akad. Nauk. Ser. Math. 3, 355 (1937)
- [33] M. Avrami, J. Chem. Phys. 8, 212 (1940)
- [34] V. Shur, E. Rumyantsev, S. Makarov, J. Appl. Phys. 84, 445 (1998)
- [35] V. Shur, E. Rumyantsev, Ferroelectrics 151, 171 (1994)
- [36] A. K. Tagantsev, I. Stolichnov, N. Setter, Physical Review B 66, 214109 (2002)
- [37] O. Lohse et al., Journal of Applied Physics 89, 2332 (2001)
- [38] X.J. Lou, J. Phys: Condes. Matter 21 (2009) 012307
- [39] Y. W. So et al., Applied Physics Letters 86, 092905 (2005)
- [40] J. Y. Jo, H.S. Han, J.G. Yoon, T.K. Song, S.H. Kim, T.W. Noh, Phys. Rev. Lett. 99, 267602 (2007)
- [41] M. Vopsaroiu, J. Blackburn, M. G. Cain, P. M. Weaver, Phys. Rev. B, vol. 82, 024109 (2010)
- [42] M. Vopsaroiu, P.M. Weaver, M.G. Cain, M.J. Reece, K.B. Chong, IEEE Transactions on Ultrasonics, Ferroelectrics, and Frequency Control, vol. 58, no. 9, 1867-1873 (2011)
- [43] Y. Zhang, X. L. Zhong, M. Vopson, J. B. Wang, Y. C. Zhou, J. Appl. Phys. 112, 014112 (2012)
- [44] H. J. Kreuzer, Nonequilibrium Thermodynamics and its Statistical Foundations, Oxford University Press, Oxford, (1981) ch. 10
- [45] M.D. Glinchuka,, E.A. Eliseeva, V.A. Stephanovich, Physica B 322 (2002) 356–370
- [46] H. He, X. Tan, Phys. Rev. B 72, 024102 (2005).

Acknowledgements

Confidential

MV acknowledges that the equipment used in this work was funded by the University of Portsmouth, Faculty of Science and XT would like to acknowledge that this work was supported by the National Science Foundation (NSF) through Grant DMR-1465254.